Hindawi Publishing Corporation
International Journal of Photoenergy
Volume 2010, Article ID 105878, 7 pages
doi:10.1155/2010/105878

Research Article

Barium Staminate as Semiconductor Working Electrodes for Dye-Sensitized Solar Cells

Fu-an Guo, Guoqiang Li, and Weifeng Zhang

Key Laboratory of Photovoltaic Materials of Henan Province, School of Physics and Electronics, Henan University, Kaifeng 475001, China

Correspondence should be addressed to Weifeng Zhang, wfzhang6@163.com

Received 2 January 2010; Revised 4 April 2010; Accepted 20 April 2010

Academic Editor: David Lee Phillips

Dye-sensitized solar cells (DSSCs) are fabricated with perovskite-type $BaSnO_3$ as the photoelectrode materials. Different preparation methods including coprecipitation, hydrothermal, and solid state reaction are employed to synthesize $BaSnO_3$ particles to optimize the photoelectric activities of electrode materials. The photoelectric properties of $BaSnO_3$ particles and the performances of DSSCs are investigated by surface photovoltage spectroscopy and current-voltage measurements. The light-to-electricity conversion of 1.1% is preliminarily reached on the DSSC made of the coprecipitation-derived $BaSnO_3$ particles. Large current density of hole injection into the HOMO level of N719 dye from the valence band of $BaSnO_3$ and reduced photogenerated charge recombination in $BaSnO_3$ could be responsible for the observed solar cell performance of the DSSC fabricated from the coprecipitation-derived $BaSnO_3$ particles.

1. Introduction

Dye-sensitized solar cells (DSSCs) have attracted increasing interest due to their potential low cost and simple preparation procedure contrast to the conventional silicon cells [1]. Since Regan and Grätzel have reported an impressive energy conversion efficiency of 7.9% for mesoporous TiO_2, DSSCs are being very extensively investigated [2]. The development of the promising photovoltaic device architectures has been well made by considering several factors, for example, (i) the synthesis of light capturing antennas [3, 4], (ii) the use of I^-/I_3^- redox couples in an appropriate medium, and (iii) the preparation of thin film electrodes using various materials [5, 6]. For the last one, some semiconductors have been applied to built new structures and avoid the oxidation of dye, such as ZnO, WO_3, In_2O_3, Nb_2O_5, SnO_2, $SrTiO_3$ and Zn_2SnO_4, and so forth [7–12].

In the fabrication of DSSCs, the band energy levels of the semiconductor must match with those of dye molecules to improve the separation of photogenerated charges and minimize their recombination [13]. In addition, the surface microstructures, particle sizes and shapes, doping concentration, porosity, and film thickness of semiconductors must also be considered and optimized. Perovskite structured $BaSnO_3$ is an n-type semiconducting material with a band gap of 3.1 eV [14]. It has been widely investigated on its dielectric, thermal, and photocatalytic properties as an important ceramic material [15]. In the previous work, we have demonstrated that the photogenerated electrons can be injected into the conduction band of $BaSnO_3$ from the excited $(Bu_4N)_2(Ru)(dcbpyH)_2(NCS)_2$ (N719) because of the energy level matching between the excited dye molecules and the conduction band state of $BaSnO_3$, suggesting a possible application of $BaSnO_3$ in DSSCs [16]. In this work, we employed the different preparation methods such as coprecipitation (CP), hydrothermal (HT) process and solid state reaction (SSR) to prepare three kinds of $BaSnO_3$ particles, which are simply called the CP, HT, and SSR $BaSnO_3$ particles for convenience, respectively, and then assemble DSSCs using them as the working photoelectrodes. The cell made up of the CP $BaSnO_3$ particles shows the best photovoltaic performance among these three cells. Based on the analysis of the dye loading and surface photovoltage spectroscopy for the dye-sensitized electrode materials, the best performance is probably due to the highest loading amount of dye and best interaction between the semiconductor and dye.

2. Experimental Section

2.1. Preparation of Samples. (1) Coprecipitation: appropriate amounts of $SnCl_4 \cdot 5H_2O$ and $Ba(CH_3COO)_2$ were separately dissolved in deionized water. After continuous stirring for 20 minutes, a quantitative volume of aqueous NaOH solution was added into the mixture solution to form a precipitate. The precipitate was filtered and washed with deionized water for several times, and then dried at 80°C and sequently annealed at 900°C for 5 hours to obtain the white CP $BaSnO_3$ particles. (2) Hydrothermal process: An aqueous $Na_2SnO_4 \cdot xH_2O$ solution was mixed with an aqueous $Ba(CH_3COO)_2$ solution. After magnetic stirring for 1 hour, the resulting mixture was transferred into a Teflon-lined stainless steel autoclave and maintained at 180°C for 12 hours, leading to the precipitation of $BaSn(OH)_6 \cdot 3H_2O$. The precipitation was converted to the HT $BaSnO_3$ particles when it was annealed at 900°C for 5 hours in air [17]. (3) Solid state reaction: the SSR $BaSnO_3$ particles were prepared by a conventional solid state reaction through sintering $BaCO_3$ and SnO_2 at 1400°C for 5 hours [14]. The N719-sensitized $BaSnO_3$ samples were prepared by, respectively, impregnating 0.2 ml ethanol solution of N719 (5×10^{-4} mol/L) into 0.3 g $BaSnO_3$ particles.

2.2. Assembling of DSSCs. The colloidal suspension was obtained via dissolving 1.2 g $BaSnO_3$ particles, 0.042 mL acetylacetone and 0.2 mL detergent (Triton X-100, Aldrich) in deionized water of 2 mL. Thin porous $BaSnO_3$ thin films were prepared on the fluorine-doped tin oxide (FTO) glass substrate ($15\,\Omega \cdot cm^{-2}$) by the doctor-blade technique with a tape as a spacer ($\approx 50\,\mu$m thick), followed by heating at 450°C for 30 minutes in air to eliminate organic compounds. The $BaSnO_3$ film thickness was about 10 μm. When cooled down at about 110°C, they were immersed into a 5×10^{-4} M solution of N719 in anhydrous ethanol for 24 hours. The dye-covered $BaSnO_3$ electrode and Pt-counter electrode (Heptachroma, China) were assembled into a sandwich type cell. A typical electrolyte (containing 0.6 M 1, 2-Dimethyl-3-propylimidazolium iodide (DMPII), 0.05 M I_2 and 0.1 M LiI in acetonitrile) was introduced into the interelectrode [18].

2.3. Characterization and Photoelectric Measurements. X-ray diffraction (XRD) patterns were recorded on a DX-2500 diffractometer (Fangyuan, Dandong) with Cu Kα radiation ($\lambda = 0.154145$ nm). Morphology and film thickness were measured by scanning electron microscope (SEM, JSM5600LV, JEOL, Japan). The surface area of the samples was determined by BET measurements (Micromeritics-3000, micrometrics, USA) on nitrogen adsorption at 77 K after the pretreatment at 573 K for 2 hours. Surface photovoltage (SPV) spectroscopy measurements were carried out with a home-built apparatus which consisted of a xenon lamp (CHF XQ500W, Beijing Trusttech Co. Ltd., China), a double-grating monochromator (Zolix SP500), a lock-in amplifier (SR830-DSP), and a light chopper (SR540). Diffuse reflectance spectra were collected with a UV-vis spectrophotometer (Varian Cary 5000) and transformed to the absorption spectra according to the Kubelka-Munk relationship. Current-voltage characteristics of the DSSCs were measured by an electrochemical workstation (CHI660B, China). The xenon lamp (CHF XQ500W, Trusttech, China) was used as the light source and its incident light intensity was measured by Radiation Meter (FZ-A, Beijing Normal University, China).

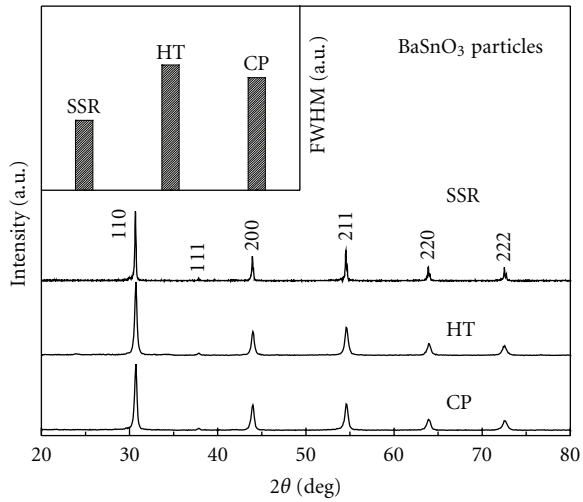

Figure 1: XRD patterns of the CP, HT, and SSR $BaSnO_3$ particles. The inset shows the FWHM of the three samples.

3. Results and Discussion

3.1. Crystal Structure and Grain Size. The XRD patterns of $BaSnO_3$ particles prepared by different methods are shown in Figure 1. They can be indexed as cubic barium stannate (JCPDS No. 15-0780). The lattice parameters estimated by a least squares match for the CP, HT, and SSR $BaSnO_3$ are 0.4116(5), 0.4114(6), and 0.4118(4) nm, respectively, being in good agreement with the reported value of 0.4114 nm [14]. The full width at half-maximum (FWHM) of the strongest (110) diffraction peak is displayed in the inset of Figure 1. The particle size is calculated using the Debye-Scherrer's law, $D = K\lambda/\beta \cos\theta$, where D is the particle diameter, K a constant, λ the wavelength of Cu Kα radiation in Å, β the full width at half-maximum (FWHM) in radians, and θ the scattering angle [19]. The estimated particle sizes for the CP, HT, and SSR $BaSnO_3$ are 26, 23, and 53 nm, respectively.

SEM images of $BaSnO_3$ particles synthesized via different routes were shown in Figures 2(a)–2(c). The SSR sample particles (Figure 2a) have a size distribution in the range of 0.3–1.1 μm and a specific surface area of 1.78 $m^2 \cdot g^{-1}$ measured by BET instrument. From Figure 2(b) and 2(c), the particles of CP and HT samples have smaller size and more aggregation compared with the SSR sample. The BET surface areas of CP and HT samples are 5.47 and 7.12 $m^2 \cdot g^{-1}$, respectively. They are both larger than that of the SSR sample. However, the surface areas of the three samples are all much smaller compared with that of traditional TiO_2

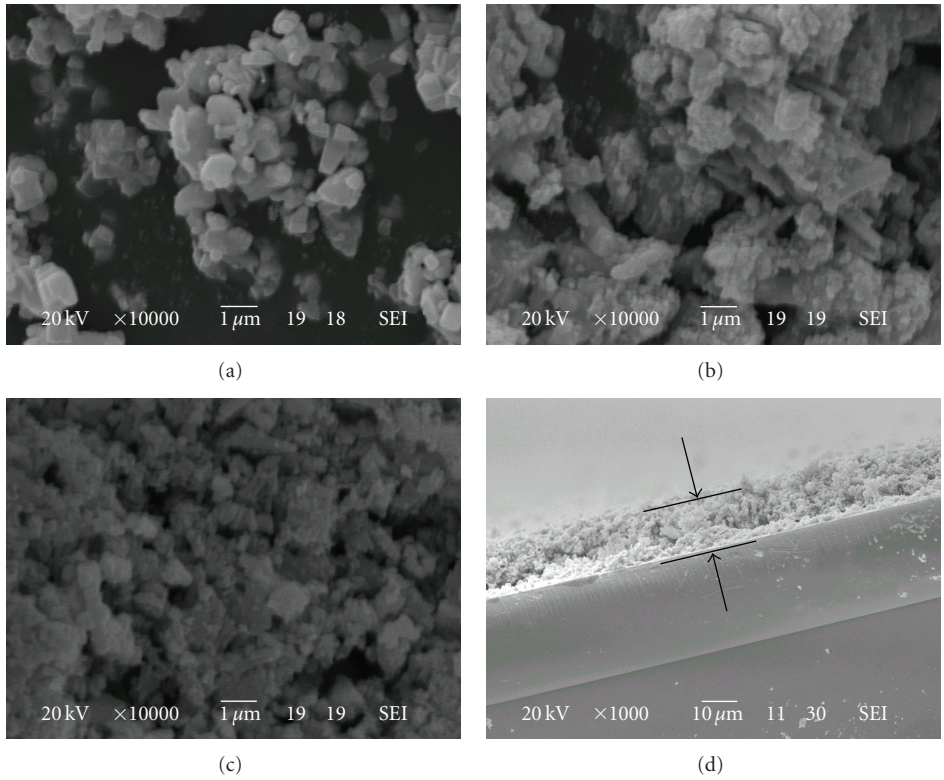

Figure 2: SEM images of $BaSnO_3$ powders prepared by different particles: (a) CP, (b) HT, and (c) SSR. (d) Cross-section of a 15 μm thick $BaSnO_3$ film electrode.

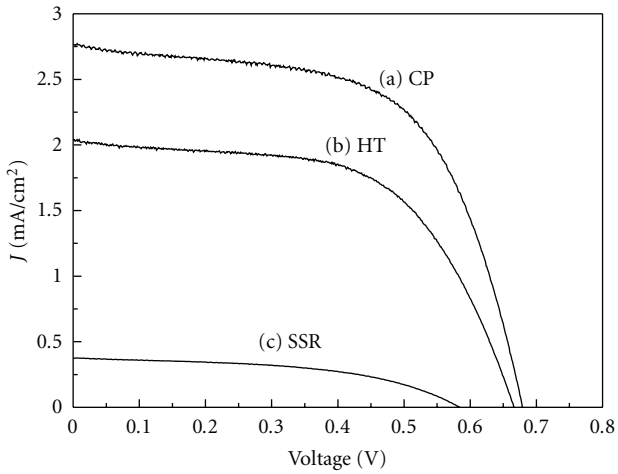

Figure 3: J-V curves of the cells prepared by different particles: (a) CP, (b) HT, and (c) SSR.

(e.g., 77 $m^2 \cdot g^{-1}$) [20]. Figure 2(d) shows the cross-section of a 15 μm thick $BaSnO_3$ film sintered at 450°C for 30 minutes in air, coated on conducting FTO glass substrates.

3.2. Photovoltaic Performance of Cells. The three dye-sensitized $BaSnO_3$ electrodes were used as the working electrodes in sandwich solar cells. Figure 3 the I-V characteristics for 0.4 cm^2 $BaSnO_3$ open cell under the light irradiation of 100 mW $\cdot$ cm^{-2} (measured by Radiation Meter). All the samples exhibit a typical behavior of the I-V curve for DSSCs. The open-circuit voltage V_{OC} and the short-circuit current density J_{SC} for the CP, HT, and SSR $BaSnO_3$ are 680 mV and 2.77 mA $\cdot$ cm^{-2}, 670 mV and 2.04 mA $\cdot$ cm^{-2}, 580 mV and 0.37 mA $\cdot$ cm^{-2}, respectively. The fill factor ff, which is defined as $P_{max}/(V_{OC}\, J_{SC})$, where P_{max} is the maximum power output, for the CP, HT, and SSR samples are calculated to be 60%, 59%, and 47%, respectively. The energy conversion efficiency under white-light irradiation can be obtained from the following equation:

$$\eta(\%) = \frac{J_{sc}[\mathrm{mAcm^{-2}}] \times V_{oc}(V) \times ff}{I_0[\mathrm{mWcm^{-2}}]} \times 100, \qquad (1)$$

where I_0 is incident light intensity. The energy conversion efficiency for the CP, HT, and SSR samples are 1.1%, 0.8%, and 0.1%, respectively. It is evident that the cell made of the CP $BaSnO_3$particles exhibits the largest value of J_{SC} and V_{OC} among these three samples. The variation trend of V_{OC} is the same as that of J_{SC}, that is, CP > HT > SSR. The difference of cell properties for the different $BaSnO_3$ particles might be related to the amounts of adsorbed dye on the three electrodes. The amounts of adsorbed dye can be evaluated using optical absorption measurements.

3.3. Optical Absorption Property. Figure 4 shows UV-vis absorption spectra for the CP and N719-sensitized CP particles at room temperature. The pristine $BaSnO_3$ exhibits

Table 1: The parameters of the $BaSnO_3$ electrode and PV performance of the DSSCs using different $BaSnO_3$ particles.

Sample	V_{OC} (V)	J_{SC} (mA · cm^{-2})	*ff*	Efficiency (%)	BET area (m^2 · g^{-1})	A_{dye} (on the film) (mol · cm^{-2})
CP	0.68	2.77	0.60	1.1	5.47	2.17 E^{-7}
HT	0.67	2.04	0.59	0.8	7.12	1.63 E^{-7}
SSR	0.58	0.37	0.47	0.1	1.78	1.08 E^{-7}

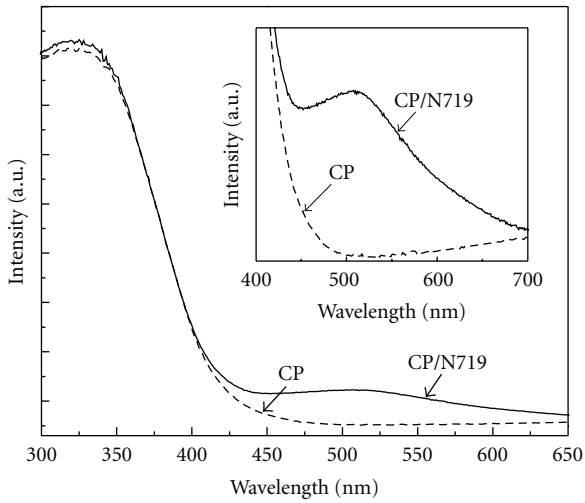

Figure 4: UV-vis absorption spectra of CP sample and N719/CP composites.

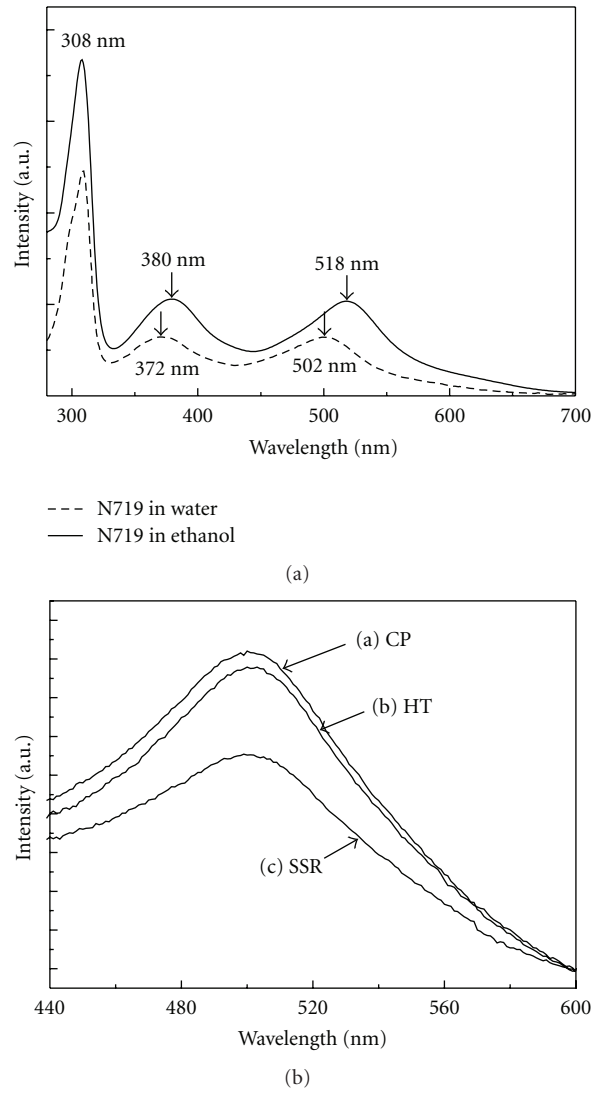

Figure 5: (a) Absorption spectra of N719 in different solvents. (b) UV-vis absorption spectra of NaOH aqueous solution containing the desorbed dye from the surface of the three $BaSnO_3$ films: CP (curve a), HT (curve b), and SSR (curve c).

an intense absorption band with a steep edge at ~400 nm (corresponding to 3.1 eV in energy) [16]. The optical absorption in the wavelength region shorter than 400 nm is mainly attributed to the electron transition from the top of the valence band to the bottom of the conduction band (band-to-band transition, O 2p → Sn 5s) [21]. After the $BaSnO_3$ particles are adsorbed with N719 molecules, a new absorption band at the peak of 515 nm emerges in the visible region, which is caused by the intraligand transitions (π-π^*) of N719 molecules.

The amount of adsorbed dye determines the number of photoexcited electrons by visible light in the N719-sensitized $BaSnO_3$ system, thus we examined the amount of adsorbed dye by using UV-vis spectroscopy [21], where the N719 dye was desorbed using a 10^{-4} M aqueous NaOH solution from the surfaces of the three $BaSnO_3$ films. Figure 5(a) illustrates the UV-vis absorption spectra of N719 in different solvents (H_2O and ethanol). The band at 518 nm is assigned to the metal-to-ligand charge-transfer of the dye in ethanol, and it shifts to shorter wavelength after the dye is dissolved in water. This effect is due to the H-bonding of solvent molecules to the electron pair of the thiocyanate sulfur, which was discussed in detail in a review article by Pérez et al. [22].

Figure 5(b) shows the optical absorption spectra of the NaOH solutions containing the desorbed dye from the surface of the three samples in the wavelength range from 440 to 600 nm. The absorption band at ~500 nm results from the light absorption of N719. Obviously, the order of the amount of the adsorbed dye of $BaSnO_3$ films are CP > HT > SSR, which is consistent with that of the photocurrent density. In general, the more the amount of dye adsorption, the more the light harvest, thus giving rise to the larger photocurrent density [23]. Therefore, the difference in the photocurrent densities for the three DSSCs is associated with the different amount of adsorbed N719 dye on the surface of the $BaSnO_3$ particles prepared using different methods. Table 1 summarizes BET specific surface

area, cell performances, and amount of adsorbed dyes of the $BaSnO_3$ electrodes for each sample.

3.4. Surface Photoelectric Property. The SPV spectroscopy is a well-established nondestructive and very sensitive characterization method to detect the change of charge distribution on a functional semiconductor surface. It has been successfully employed for the quantitative determination of the energetic and dynamic parameters of surface states in many semiconductor materials. It is also versatile for investigating charge-transfer phenomena in photostimulated surface interactions, dye sensitization processes, and particularly in photovoltaic devices [24, 25]. The SPV measurements (inset of Figure 6) were carried out with a solid junction photovoltaic cell (ITO/sample/ITO) structure. During the process of SPV measurement, the ITO glass can strongly absorb the light with the wavelength lower than 300 nm, which results in a corresponding weak or even no SPV signal.

The SPV of the unsensitized and N719-sensitized CP $BaSnO_3$ are presented in Figure 6. It can be seen that a pronounced SPV response band appears at ~354 nm, which can be mainly ascribed to the electron transition from O 2p to Sn 5s orbitals. Compared with the SPV of pristine $BaSnO_3$, the photovoltaic response band in the range of 300–450 nm is enhanced remarkably after N719 was adsorbed. Such an observation indicates that the recombination of the photogenerated electron-hole pairs in $BaSnO_3$ is efficiently suppressed because the holes in the excited $BaSnO_3$ particles are injected into the HOMO level of dye from the valence band of $BaSnO_3$ [26]. A new photovoltaic response band appearing in the visible region of 450–650 nm is obviously associated with the light absorption of N719 molecules and results from the electron injection from the excited dye into the conduction band of $BaSnO_3$.

Figure 7 shows the SPV spectra of the three N719-sensitized $BaSnO_3$ samples. As mentioned above, the photovoltaic response band in the range of 450–650 nm is assigned to the electron injection from the excited dye to the conduction band of $BaSnO_3$. The BET surface areas of the CP, HT, and SSR particles are 5.47, 7.12, and 1.78 $m^2 \cdot g^{-1}$, respectively. The amount of dye adsorption is closely related to the surface area of a semiconductor particle, and thus the SPV response is also affected. The SSR sample has the smallest surface area and the least absorption dye, so the SPV response band in the range of 450–650 nm of the N719/SSR is the weakest in Figure 7. However, the SPV response band from 450 to 650 nm of N719/CP is stronger than that of N719/HT, while the HT sample has a bigger surface area and thus more dye adsorption. Therefore, there are other factors to affect the SPV signal intensity. As we know, the SPV response of the composite is significantly affected by the transfer of photoinduced charges from the dye to the semiconductor as well as the interaction between them [16]. It is reasonable to deduce that the strong SPV response band in the range of 450–650 nm of the N719/CP sample is attributed to the strong interaction between the CP particles and N719 molecules [18, 27].

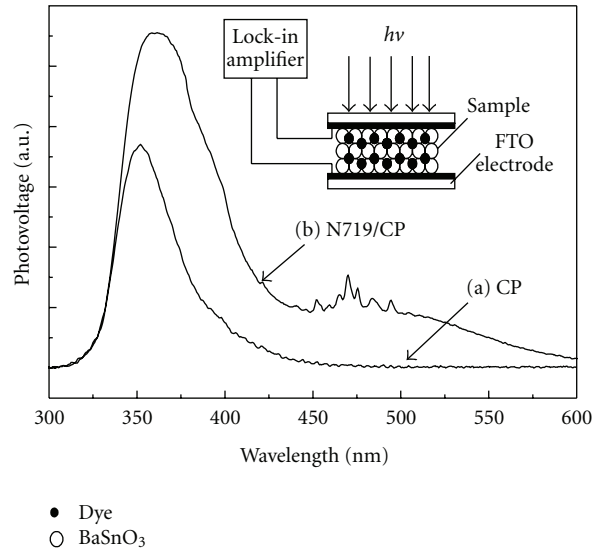

Figure 6: Surface photovoltage spectra of CP (curve a) and N719/CP samples (curve b). Inset: a schematic diagram of a photovoltage measurement.

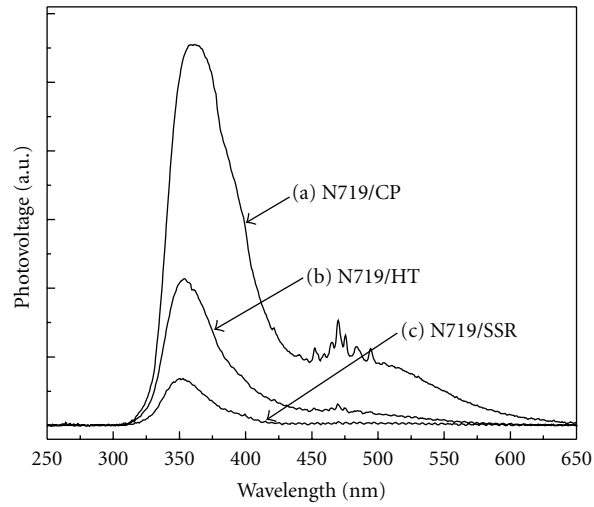

Figure 7: Surface photovoltage spectra of N719/CP (curve a) sample, N719/HT sample (curve b), and N719/SSR sample (curve c).

The strong SPV response for the sample N719/CP and the sufficient dye adsorption onto the CP film bring the best photoelectric performance of the CP-DSSC. However, the photoelectric conversion efficiency of cells obtained in the present work is very low. The low photovoltaic performance might be ascribed to the aggregation, small specific surface area of $BaSnO_3$ particles and unsuited film thickness. To improve the photoelectric performance of the $BaSnO_3$ DSSCs, the electrode preparation of $BaSnO_3$ particles is being optimized by using new synthesis techniques, and the related work is in progress.

4. Conclusions

N719 dye-sensitized solar cells based on semiconducting $BaSnO_3$ particles synthesized by different methods were fabricated and investigated on their photoelectric properties. The cell of coprecipitation-derived $BaSnO_3$ particles exhibits the best photovoltaic performance, which is attributed to sufficient dye adsorption and good electronic interaction between $BaSnO_3$ and dye. The results suggest that the controlling synthesis process would be a key strategy to apply appropriate material for dye-sensitized solar cells.

Acknowledgments

This work was supported by the Project of Cultivating Innovative Talents for Colleges & Universities of Henan Province (2002006) and the Natural Science Foundation of Department of Education of Henan Province (2009B48003) and the Key Technologies R & D Program of Henan Province (092102210005).

References

[1] M. Grätzel, "Conversion of sunlight to electric power by nanocrystalline dye-sensitized solar cells," *Journal of Photochemistry and Photobiology A*, vol. 164, no. 1–3, pp. 3–14, 2004.

[2] B. O'Regan and M. Grätzel, "A low-cost, high-efficiency solar cell based on dye-sensitized colloidal TiO_2 films," *Nature*, vol. 353, no. 6346, pp. 737–740, 1991.

[3] P. Falaras, "Synergetic effect of carboxylic acid functional groups and fractal surface characteristics for efficient dye sensitization of titanium oxide," *Solar Energy Materials & Solar Cells*, vol. 53, no. 1-2, pp. 163–175, 1998.

[4] P. Falaras, M. Grätzel, A. Hugoy-Le Goff, M. Nazeeruddin, and E. Vrachnou, "Dye sensitization of TiO_2 surfaces studied by Raman spectroscopy," *Journal of the Electrochemical Society*, vol. 140, no. 6, pp. L92–L94, 1993.

[5] A. Kay and M. Grätzel, "Dye-sensitized core-shell nanocrystals: improved efficiency of mesoporous tin oxide electrodes coated with a thin layer of an insulating oxide," *Chemistry of Materials*, vol. 14, no. 7, pp. 2930–2935, 2002.

[6] K. Hara, T. Horiguchi, T. Kinoshita, K. Sayama, H. Sugihara, and H. Arakawa, "Highly efficient photon-to-electron conversion with mercurochrome-sensitized nanoporous oxide semiconductor solar cells," *Solar Energy Materials & Solar Cells*, vol. 64, no. 2, pp. 115–134, 2000.

[7] A. N. M. Green, E. Palomares, S. A. Haque, J. M. Kroon, and J. R. Durrant, "Charge transport versus recombination in dye-sensitized solar cells employing nanocrystalline TiO_2 and SnO_2 films," *Journal of Physical Chemistry B*, vol. 109, no. 25, pp. 12525–12533, 2005.

[8] K. Sayama, H. Sugihara, and H. Arakawa, "Photoelectrochemical properties of a porous Nb_2O_3 electrode sensitized by a ruthenium dye," *Chemistry of Materials*, vol. 10, no. 12, pp. 3825–3832, 1998.

[9] P. Guo and M. A. Aegerter, "RU(II) sensitized Nb_2O_3 solar cell made by the sol-gel process," *Thin Solid Films*, vol. 351, no. 1-2, pp. 290–294, 1999.

[10] M. Quintana, T. Edvinsson, A. Hagfeldt, and G. Boschloo, "Comparison of dye-sensitized ZnO and TiO_2 solar cells: studies of charge transport and carrier lifetime," *Journal of Physical Chemistry C*, vol. 111, no. 2, pp. 1035–1041, 2007.

[11] B. Tan, E. Toman, Y. Li, and Y. Wu, "Zinc stannate (Zn_2SnO_4) dye-sensitized solar cells," *Journal of the American Chemical Society*, vol. 129, no. 14, pp. 4162–4163, 2007.

[12] S. Burnside, J.-E. Moser, K. Brooks, M. Grätzel, and D. Cahen, "Nanocrystalline mesoporous strontium titanate as photoelectrode material for photosensitized solar devices: increasing photovoltage through flatband potential engineering," *Journal of Physical Chemistry B*, vol. 103, no. 43, pp. 9328–9332, 1999.

[13] J. B. Baxter and E. S. Aydil, "Dye-sensitized solar cells based on semiconductor morphologies with ZnO nanowires," *Solar Energy Materials & Solar Cells*, vol. 90, no. 5, pp. 607–622, 2006.

[14] W. Zhang, J. Tang, and J. Ye, "Structural, photocatalytic, and photophysical properties of perovskite $MSnO_3$ (M = Ca, Sr, and Ba) photocatalysts," *Journal of Materials Research*, vol. 22, no. 7, pp. 1859–1871, 2007.

[15] T. Maekawa, K. Kurosaki, and S. Yamanaka, "Thermal and mechanical properties of polycrystalline $BaSnO_3$," *Journal of Alloys and Compounds*, vol. 416, no. 1-2, pp. 214–217, 2006.

[16] Y. Zhang, H. Zhang, Y. Wang, and W. F. Zhang, "Efficient visible spectrum sensitization of $BaSnO_3$ nanoparticles with N719," *Journal of Physical Chemistry C*, vol. 112, no. 23, pp. 8553–8557, 2008.

[17] T. R. N. Kutty and R. Vivekanadan, "$BaSnO_3$ fine powders from hydrothermal preparations," *Materials Research Bulletin*, vol. 22, no. 11, pp. 1457–1465, 1987.

[18] Y. Fukai, Y. Kondo, S. Mori, and E. Suzuki, "Highly efficient dye-sensitized SnO_2 solar cells having sufficient electron diffusion length," *Electrochemistry Communications*, vol. 9, no. 7, pp. 1439–1443, 2007.

[19] P. Jha, P. R. Arya, and A. K. Ganguli, "Dielectric properties of lead zirconium titanates with nanometer size grains synthesized by the citrate precursor route," *Materials Chemistry and Physics*, vol. 82, no. 2, pp. 355–361, 2003.

[20] S. Nakade, Y. Saito, and W. Kubo et al., "Enhancement of electron transport in nano-porous TiO_2 electrodes by dye adsorption," *Electrochemistry Communications*, vol. 5, no. 9, pp. 804–808, 2003.

[21] D. Cahen, G. Hodes, M. Grätzel, J. F. Guillemoles, and I. Riess, "Nature of photovoltaic action in dye-sensitized solar cells," *Journal of Physical Chemistry B*, vol. 104, no. 9, pp. 2053–2059, 2000.

[22] C. Pérez León, L. Kador, B. Peng, and M. Thelakkat, "Influence of the solvent on the surface-enhanced Raman spectra of Ruthenium(II) Bipyridyl complexes," *Journal of Physical Chemistry B*, vol. 109, no. 12, pp. 5783–5789, 2005.

[23] G. Schlichthörl, S. Y. Huang, J. Sprague, and A. J. Frank, "Band edge movement and recombination kinetics in dye-sensitized nanocrystalline TiO_2 solar cells: a study by intensity modulated photovoltage spectroscopy," *Journal of Physical Chemistry B*, vol. 101, no. 41, pp. 8141–8155, 1997.

[24] A. D. Q. Li and L. S. Li, "Photovoltage enhancement: analysis of polaron formation and charge transport at the junctions of organic polythiophene and inorganic semiconductors," *Journal of Physical Chemistry B*, vol. 108, no. 34, pp. 12842–12850, 2004.

[25] M.-H. Qi and G.-F. Liu, "Surface photovoltage, luminescence, and cyclic voltammetry on the first series of lanthanide(III) monobenzoporphyrin compound liquid crystals and relative transition metal benzoporphyrin compound liquid crystals," *Journal of Physical Chemistry B*, vol. 107, no. 31, pp. 7640–7646, 2003.

[26] L. Jing, Z. Xu, J. Shang, X. Sun, W. Cai, and H. Guo, "The preparation and characterization of ZnO ultrafine particles,"

Materials Science and Engineering A, vol. 332, no. 1-2, pp. 356–361, 2002.

[27] J.-H. Yang, W.-S. Yang, and X.-D. Chai et al., "Improved surface photovoltaic response of nanoparticulate TiO_2-pyridine derivative monolayer/n-Si(111) assembly," *Synthetic Metals*, vol. 86, no. 1, pp. 2127–2128, 1997.